Proceedings of International Mechanical Engineering Congress & Exposition
IMECE 2017
November 3-9, 2017, Tampa, USA

IMECE2017-71995

HEAT FLUX CHARACTERISTICS OF ASYMMETRICALLY HEATED AND COOLED THERMAL STIMULI

Mehdi Hojatmadani, Matthew Hardy, Ahmad Manasrah*, Rasim Guldiken, Kyle Reed
Department of Mechanical Engineering
University of South Florida
Tampa, Florida 33620
Email: kylereed@usf.edu

ABSTRACT

The human thermal response system can be manipulated by the proper combination of applied hot and cold stimuli. Previous research has shown that a sensation of constant cooling can be perceived through the application of certain patterns on the skin. Here we focus on (1) exploring the heat flux characteristics of the thermal display through computer simulations, (2) testing a hypothesis about the relationship between thermal sensation and heat flux, and (3) examining modifications of the thermal display patterns to intensify thermal sensations. To characterize the heat flux patterns of the thermal display, finite element simulations were performed using ANSYS. Simulations were done in two parts: the first examined a small subregion between heating and cooling stimuli, and the second was a larger scale examination of the heat flux profile of the thermal display. It was observed that the heat flux profiles for all thermal patterns were approximately identical. A linear relationship is derived between simulation and experimental results. This relationship was then used to determine the theoretical thermal sensations to determine which are best suited for future physical experimentation on humans.

INTRODUCTION

The human sensory receptors detect external changes in the environment and transmit signals to the brain. The brain interprets these signals and responds accordingly. Well known receptors include: chemoreceptors, mechanoreceptor and thermoreceptors. Each of these receptors are responsible for specific interactions with the environment. Chemoreceptors and mechanoreceptor are responsible for senses such as taste, smell, and touch [1, 2]. Thermoreceptors are responsible for temperature sensation as well as the control and regulation of body temperature [3]. Thermoreceptors are located throughout the skin at various depths and in various concentrations. When a thermal stimulus is present on the skin, thermoreceptors begin to fire signals to the brain. When the brain receives these signals, it interprets them as either hot or cold and responds accordingly. The interpretations of thermal stimuli by the brain affect other areas of human perception as well. For example, skin temperature has an affect on vibrotactile perception [4].

Thermoreceptors are divided into warm and cold receptors [5] with cold receptors being more prevalent in the human skin than warm receptors at a ratio of thirty-to-one [6]. Additionally, warm and cold receptors respond to different rates of temperature change [7] and are activated at different ranges of temperatures. Warm thermoreceptors are active in the range from 30°C to 45°C. Cold thermoreceptors are active in the range of decreasing temperatures from 30°C to 18°C. Below 18°C and above 45°C, thermal sensation transitions to a feeling of pain which is transmitted through receptors called nocioceptors [8]. The sensation of pain has been shown to be directly related to the magnitude of the temperature difference even when hot and cold temperatures are well below the pain threshold [9]. As the area of thermal stimulation increases, the perceptible threshold decreases [7].

Kenshalo [7, 10] showed that the rate of temperature change determines the perceivable thermal threshold. Additionally,

*A. Manasrah is currently affiliated with Al-Zaytoonah University of Jordan.

thermoreceptors respond to decreasing temperatures much quicker than increasing temperatures [11, 12]. Manasrah et al. showed that a perceived sense of constant cooling [13] and constant heating [14] could be achieved through the use of asymmetrically heating and cooling thermal actuators. However, thermal perception is not based on absolute temperature but on temperature difference or heat flux. Therefore, the primary contribution of this paper is the development of a relationship between the thermal perception of the patterns used in the physical experiment and the heat flux values calculated from the simulations.

BACKGROUND

Heat Flux

Heat flux is defined as the rate of heat transfer per unit area, i.e., W/m^2. The equation for heat flux can be written as:

$$q''_n = -k\frac{dT}{dm} \tag{1}$$

where q''_n is the heat flux per unit area in the direction normal to the surface through which heat is being conducted, k is the thermal conductivity unique to the material and $\frac{dT}{dm}$ is the directional temperature gradient, where m represents either x, y or z. The driving force behind heat flux is the temperature gradient within an object. The temperature gradient is a function of the initial temperature of the object and the boundary temperatures of the object, due either to an applied temperature, convecting fluid, or other generation source. Heat flux is driven by the temperature gradient of an object. However, certain objects can feel colder than others even if both are at an identical temperature. This phenomenon is due to the thermal conductivity of a material, k with units W/m*K. In solid substances, heat is conducted through the vibration of the lattice structure of the material, creating structural waves known as phonons [15].

The transient model of the heat flow equation can be represented in mathematical form as:

$$\nabla * (k\nabla T) + g = \rho c\frac{dT}{dt} \tag{2}$$

It is from this equation that the heat flow characteristics of the system presented in this paper are derived. Even with some simplifying assumptions, such as eliminating the internal generation term, this equation is too laborious and time consuming to develop solutions for the number of unique systems involved. This is what necessitates the need for computer simulation software.

Simulated Models

Engineering professionals have been working for decades to develop more accurate methods for solving computer simulations. Meshes can range from coarse to very fine. The mesh must comply with certain metrics such as quality, skewness and aspect ratio that ensure the quality of the solution.

Common simulation methods include equation-based, agent-based, and Monte Carlo simulations. Equation based simulations are those that use natural principles that describe the physical behavior of a system. Agent Based Modeling (ABM) simulations are generally used to study how multiple objects, governed by different rules, interact with each other over time. Monte Carlo (MC) simulations use probability distributions to develop approximate solutions to problems. MC simulations are generally used as a supplemental verification and not necessarily as the primary tool for studying a system [16].

Quality Criteria

The validity of simulation results depend largely on the parameters selected prior to initializing the simulation. Orthogonal element quality, element aspect ratio and element skewness are a few of the metrics used to validate the quality of model results. Orthogonal element quality is defined relative to adjacent cells. This metric is a dot product of vectors that describe element centroids and face normal vectors. Orthogonal quality defines the uniformity of a generated mesh. The aspect ratio of an element is defined as the ratio of the longest side of an element to the shortest side of an element [17]. The aspect ratio of a generated element is compared with the idealized shape, either a unit square or an equilateral triangle. The idealized version of these shapes has a value of one. The further from the idealized aspect ratio, the more inaccurate a solution becomes. The skewness of an element is a measure of angular deviation from an idealized shape [18, 19].

Three quantities are necessary to define the orthogonal quality of a mesh: the area vector of a cell face, A_i, the centroid of a cells face, f_i, and the centroid of the adjacent cell, c_i. A_i is the vector, normal to face i of a cell, scaled relative to its area. f_i is a vector from the centroid of the element to the centroid of face i. c_i is the vector from the centroid of the element to the centroid of the element adjacent to face i. Two dot product calculations are conducted from these values and the minimum value is taken to be orthogonal quality for the element being evaluated.

$$min\left[\frac{A_i * f_i}{\|A_i\| * \|f_i\|}, \frac{A_i * c_i}{\|A_i\| * \|c_i\|}\right] \tag{3}$$

ANSYS defines the orthogonal quality as: $0-0.001$ as unacceptable, $0.001-0.14$ as bad, $0.14-0.20$ as acceptable, $0.20-0.69$ as good, $0.70-0.79$ as very good and $0.98-1.00$ as excellent [20]. The aspect ratio of an element can be defined in two ways. The first is the ratio of the largest length of an element to the smallest length of an element for regular element shapes [17]. The second is the ratio of the

radius of a circle circumscribed around an element and the radius of a circle inscribed inside an element for irregularly shaped elements [21]. Aspect ratio is an important metric due to the processing requirements of numerical simulation algorithms. These algorithms perform the same operations on multiple parts of the data simultaneously. This necessitates equal sizing of elements in order to more accurately calculate the information at each step. The decomposition of a model is used to construct preconditioners which represent the initial problem assumptions [22]. The shape of the elements heavily influences the quality of the preconditioners and it is for this reason that the aspect ratio is such an import metric for generating a quality solution. Additionally, the quality of model preconditioners affect the solution time of a simulation [21]. Skewness is calculated based on both the maximum angular value, θ_{max}, minimum angular value, θ_{min}, and the idealized angular value, θ_e.

$$max\left[\frac{\theta_{max}-\theta_e}{180-\theta_e}, \frac{\theta_e-\theta_{min}}{\theta_e}\right] \tag{4}$$

ANSYS skewness values are categorized in the following way: $0-0.25$ are considered excellent, $0.25-0.50$ are very good, $0.5-0.80$ are good, $0.80-0.94$ are acceptable, $0.94-0.97$ are bad and $0.98-1.00$ are unacceptable [20].

HEAT FLUX DURING HEATING/COOLING CYCLES

Three sets of simulations are performed throughout this paper. First, a preliminary examination of the isolated heating and cooling segments is performed. Later, the experimental patterns used to achieve constant cooling are simulated in order to gain an insight on heat flux profiles seen in the skin. The last set of simulations is a new set of patterns with altered timings and spatial variations.

The physical experiment that these simulations are based on used thermal actuators (peltier devices) to control the rate of temperature change such that if a set of thermal actuators were heating at a rate below the perceptual threshold the heating *would not* be noticed. Simultaneously, if a set of actuators were cooling at a rate above the perceptual threshold this sensation *would* be noticed. In addition, the location of the cooling actuators are constantly changing. The locations of heating and cooling actuators were deliberately chosen as well. In several experiments, the patterns were ordered while in others, the patterns were systematically disordered.

The temperature profile is therefore required to hold a three/one heating cooling ratio. All timing patterns are scaled according to this with 21/7, 30/10 and 45/15 heating/cooling being the primary rates.

Heat Flux: A Theoretical Analysis

The work done by Manasrah et al. [13] demonstrated that a perception of constant cooling was possible. Additional work was done to validate the temperatures apparent in the system. This was done by creating a model of the actual experiment. The model consisted of a copper and polyurethane hollow cylinder to approximate the internal parts of the body and skin, respectively. Thermal actuators (Peltier devices) used in the actual experiments were included in the model in order to manipulate temperature.

Analytic Solution to the Heat Equation The analysis of the heat flux values present in the system will be limited to the radial direction of the hollow cylindrical coordinate system. Because the surface flux is being examined, the differential will become a delta approximation and Equation 1 becomes:

$$q''_r = -k * \frac{\Delta T}{\Delta r} \tag{5}$$

where r is the radius of the cylinder.

Isolated Heating and Cooling Segments Four distinct cases will be examined using Fourier's Law in the radial dimension. The four cases to be examined are:

1. Actuator heating over 30 seconds from skin temperature, 32°C, increases 1°C to 33°C.
2. Actuator heating over 30 seconds with its initial temperature half a degree lower than skin temperature, 31.5°C, and increase to 32.5°C.
3. Actuator cooling over 10 seconds with its initial temperature half a degree higher than skin temperature, 32.5°C, and decreases 1°C to 31.5°C.
4. Actuator cooling over 10 seconds with its initial temperature equal to skin temperature, 32°C, and decreases 1°C to 31°C.

SIMULATED HAPTIC MODEL

Two unique pieces of software were used in conjunction with each other: Solidworks for creating the physical model and ANSYS Workbench for analyzing the experiment using Finite Element Analysis. The standard model consisted of three components used in the experimental setup: a copper cylinder, a polyurethane rubber cylinder and thermal actuators known as peltier devices. The copper cylinder was in direct contact with the polyurethane cylinder. The polyurethane rubber was used as a medium to represent human skin. Polyurethane rubber was chosen because it has similar thermal properties as that of skin. A comparison between their properties can be seen in Table 1.

The copper cylinder has an inner and outer radius of 37.05 mm and 38 mm respectively. The polyurethane cylinder

TABLE 1: Thermal properties of human skin and polyurethane.

Material	Density (Kg/M^3)	Heat Capacity (J/Kg*K)	k (W/m*K)
Skin	1062	3400	0.29
Polyurethane	1200	1800	0.3

has a thickness of 2 mm leading to an inner and outer radius of 38 mm and 40 mm respectively. Two millimeters thickness was chosen because that is the approximate thickness of human forearm skin. Both the copper cylinder and the polyurethane cylinder are 304.8 mm long. The aluminum actuators have a cross-sectional area of 255 mm^2 or 15 mm x 15 mm with a thickness of 3.8 mm.

ANSYS Transient Thermal Setup

In any simulation, there is the possibility that the results may not accurately represent the physical phenomena. There are several steps and precautions required to ensure accuracy of the results. The Model section is where the actual simulation parameters are specified. This includes coordinate systems, meshing, and analysis settings. Setup and Solutions are also specified in the Model environment and generated by the software. Finally, results are the actual generated data from the simulation.

Simulation Parameters The parameters in this section are broken into three parts: Model, Transient Thermal, and Solutions. Model consists of Geometry, Coordinate System, Connections, and Mesh. Transient Thermal is comprised of: Initial Temperature and Analysis Settings. "Coordinate System" is where specific locations can be selected for analysis. This option allows the user to define an x, y and z coordinate location as well as the orientation of the coordinate system. These locations are later used to place objects known as "Probes" throughout the solid model that collect specific information at areas of interest. "Connections" is where the contact locations between different bodies is specified. "Contact Sizing" states the size of the mesh at the interface of two bodies. Under the "Transient Thermal" section, the initial temperature is specified. A total of five temperature conditions are created here: one internal temperature and four actuator temperature patterns.

Nodal Convergence Study When running simulations, an important aspect is the ability to properly mesh a model. Therefore it is desirable to determine at what mesh size the solution output becomes stable in order to balance accuracy with time to solution. In order to determine a mesh size that will produce accurate results while solving in a reasonable time, a nodal convergence study is performed. A nodal convergence study is the process of running the same simulation several times, under identical conditions and solution settings, with the only varying parameter being the mesh size. For this convergence study, the initial mesh size selected was 5 mm. The mesh size of each subsequent simulation decreased at regular intervals. Below 2 mm, the mesh size increments varied slightly and became smaller in order to gain more detailed insight into how the mesh quality was changing. Ideal characteristics include high mesh quality, low aspect ratio, and low skewness. Table 2 indicates that acceptable mesh quality appears around 2.5 mm mesh size, however, to obtain an even higher quality solution, a smaller mesh is chosen.

TABLE 2: Nodal convergence metrics

Mesh Size (mm)	Mesh Quality	Aspect Ratio	Skewness
5	0.405	4.472	0.641
4	0.422	5.096	0.613
3	0.512	3.662	0.554
2.5	0.559	3.395	0.513
2	0.622	3.408	0.432
1.8	0.640	3.252	0.423
1.5	0.640	2.725	0.429
1	0.777	2.169	0.309
0.9	0.769	2.179	0.324
0.8	0.756	2.215	0.343

It is worth to mention that difference from a 2.5 mm mesh to a 1 mm mesh was negligible and the smaller mesh was chosen for use throughout this study.

Heat Flux: A Simulated Analysis

In the following section, the four cases seen in the "Heat Flux: A Theoretical Analysis" section will be simulated through ANSYS Workbench using finite element analysis.

Numerical Method of Solving the Heat Equation ANSYS uses a consistent method for solving computational analysis using FEM. The methodology consists of three phases: preprocessing, solution, and post-processing. The preprocessing phase consists of creating and meshing the model, defining the shape function which describes the interpolation of data between nodes, developing the equations for an element, assembling the elements to describe the entire system and applying boundary conditions. The solution phase solves the set of algebraic

equations developed in the prepossessing phase in order to obtain nodal results, such as temperature. The post-processing phase utilizes the nodal results and determines the final values of interest, such as heat flux [23]. The general heat transfer relation used by ANSYS in matrix form is seen in Equation 6.

$$\rho c \frac{\partial T}{\partial t} + [L]^T [q] = \ddot{\dot{q}} \tag{6}$$

where, ρ is material density, c is heat capacity, $\frac{\partial T}{\partial t}$ is the temperature gradient in x, y and z, $[L]$ is the differential operator for x, y and z, $[q]$ is the heat flux vector in x, y and z, and $\ddot{\dot{q}}$ is the volumetric heat generation.

ANSYS uses a time integration procedure based on the generalized Euler scheme to perform time stepping operations in transient thermal simulations. The Euler method selects a time step based on the Fourier and Biot number. These two numbers are dimensionless quantities that help to define time dependent conduction problems [24, 25].

$$Fo = \frac{\alpha \Delta t}{\Delta x^2} \quad \text{and} \quad Bi = \frac{h \Delta x}{k} \tag{7}$$

where, the Fourier number is the ratio of diffusive effects to the storage rate of a body and the Biot number is the ratio of internal conduction effects to external convective effects. If the Biot number is sufficiently small, as is the case for the entirety of this study due to the lack of convection, the time step is a function of only the Fourier number. The combination of mentioned equations is the method by which ANSYS solves transient thermal simulations. Simulation results have been validated by heat flux obtained from empirical equations. These values were used by the software internally to optimize the model solution.

Heating From Skin Temperature Initially, there is a slight non-linearity in the heat flux value. This is likely due to the transient heat flow and necessity of heat to propagate into the polyurethane cylinder in order for any amount of flux to be present. Following this transient period, the expected linear profile dominates the heat flow characteristics of the segment. The data shows a final heat flux value of approximately 142 W/m^2. This results in a 5% difference between the analytic and simulation analysis.

Heating From Below Skin Temperature The analytic calculations showed an initial negative heat flux value was approximately -75 W/m^2 and the final value of 75 W/m^2. An initial non-linearity in the data is present at the beginning of the analysis but it does stabilize within the first 5 seconds.

Cooling From Above Skin Temperature In this case a trend similar to case 2 was observed with a slight non-linearity at the beginning and relative stability reached shortly after as well as some level of symmetry around zero. The heat flux values produced by ANSYS are approximately 55 W/m^2 and decrease to approximately 51 W/m^2.

Cooling From Skin Temperature Case 4 is the final cooling scenario where skin cools one degree from 32°C to 31°C over 10 seconds. An initial value of 0 W/m^2 with a linear decrease to -150 W/m^2 was observed in the analytic case.

Asymmetric Heating and Cooling Cycles

Two different sections of the cylinder models are examined for this section of the study. The first is along the centerline, under and between two actuators defined in Figure 1. The second is along the centerline, under and between all four actuators of the cylinder along the z-axis. For this simulation, the y-axis represents the radial direction, the z-axis represents the axial direction and the x-axis represents the angular direction. Cartesian directions are used since this analysis focuses on one row of actuators on the surface parallel to the cylinder centerline.

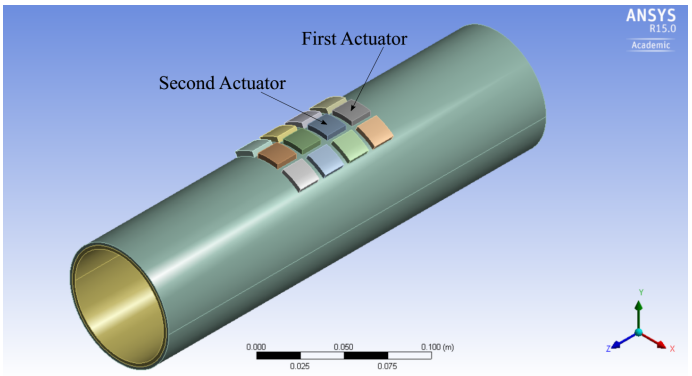

FIGURE 1: Schematic of global coordinate system orientation and actuator names in developed model. The cartesian axes are aligned with the middle row, which is the focus of this analysis.

Temporal Patterns and Spatial Patterns The setup of the original experiment determined the ratio of timing patterns. There are four rows of three adjacent actuators; one row is at its peak value of 32.5°C, one row is at its minimum value of 31.5°C and two rows are slowly heating. This leads to a ratio of 3/1 heating/cooling. All timing patterns chosen for simulation are scaled based on this ratio. The three timing patterns are 21/7 heating/cooling (0.047°C/s and 0.14°C/s), 30/10 heating/cooling

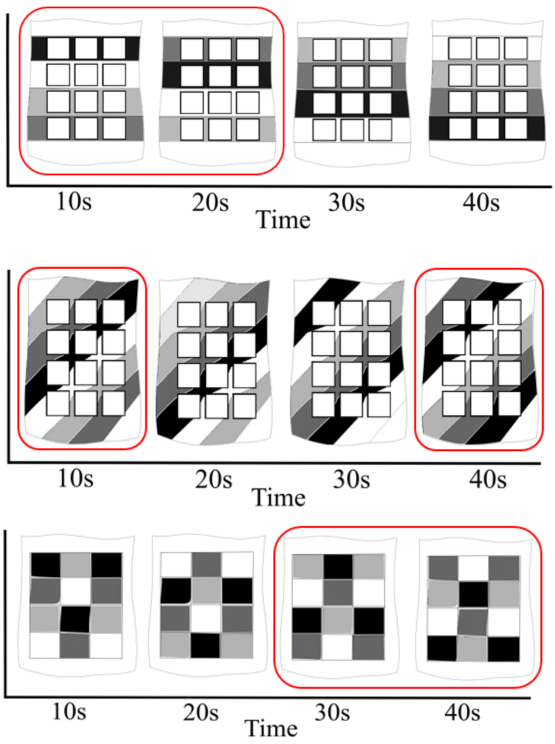

FIGURE 2: (a)The horizontal heating pattern. (b)The diagonal heating pattern. (c) The arbitrary heating pattern. The peak temperatures (black) for the area of interest are circled in red.

(0.033°C/s and 0.1°C/s) and 45/15 heating/cooling (0.022°C/s and 0.067°C/s). All timing patterns meet the requirement of being below the threshold rate for heating and above the threshold rate for cooling.

The three spatial patterns selected for simulation are horizontal, diagonal and arbitrary, as shown in Figure 2. The horizontal pattern is defined as a row of three neighboring actuators at the same location along the z-axis. As one row of actuators reaches its peak and begins cooling, the following row of actuators begins heating. The diagonal pattern is defined as three adjacent actuators in different rows along the z-axis. The corner of each actuator is in contact with the adjacent actuator corner. The arbitrary pattern consists of two actuators in the same row on either side of the centerline and one actuator on the centerline two rows ahead. Visually this can be equated to the vertices of an isosceles triangle. All of these patterns shift along the positive z axis until the fourth row of actuators is reached at which point, the pattern was started again at the first row of actuators.

Simulated Patterns Based on the time patterns and spatial patterns, nine different simulation combinations were performed. Horizontal, diagonal and arbitrary spatial patterns with temporal ratios of 21/7, 30/10 and 45/15. The time delay of each actuator segment at the beginning of the simulation causes a transient state of heat transfer. In order to eliminate any transient effects, the first 90 time step values were removed from analysis. This resulted in a total analysis time of 68 seconds for the 21/7 rate, 96 seconds for 30/10 and 145 seconds for the 45/15 rate.

Heat Flux Profile for Two Actuators Figure 3 shows the locations of the five heat flux and five temperature probes. Probe locations one and five are directly under the center of the first and second actuators. Probes two, three and four are between the first and second actuators. Two and four are located one millimeter from the edge of their adjacent actuator. Probe three is located directly at the midpoint between the first two actuators.

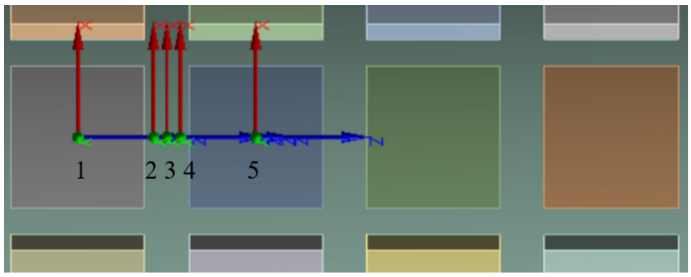

FIGURE 3: Probe locations under and between first two actuators. The five locations where heat flux data was examined for this analysis.

The heat flux difference profile is plotted based on the specific time pattern. For each set of data, the spatial pattern is held constant. The heat flux difference values in the x-direction are significantly lower than the other directions and do not exhibit substantial changes. Therefore, the x-direction values will not be investigated.

The first group to be examined is the horizontal heating pattern. Table 3 shows that at locations one and five, which represent the probes directly under the actuators, the largest value is in the y direction. This is reasonable because those areas are in closest contact with the changing temperatures and therefore experience the largest positive and largest negative heat flux values leading to the largest heat flux difference values. The heat flux values in the x and z direction for probes one and five have the smallest heat flux difference values. This is because the area surrounding the probes experience very small temperature differential and therefore very little change in heat flux.

The heat flux difference values are significantly lower at probe three for all directions when compared with probes two and four. The furthest possible distance from the heating source is 2.5mm and therefore experienced a significantly lower

TABLE 3: Heat flux difference values for the horizontal pattern. Data in y direction as well as the total magnitude for all five probe locations for horizontal pattern is shown.

Horizontal 21/7 (W/m*K)					
Probe	1	2	3	4	5
diff y	134.7	30.7	8.7	32	142.4
Horizontal 30/10 (W/m*K)					
diff y	139.1	34.1	10.8	37.3	144.6
Horizontal 45/15 (W/m*K)					
diff y	142	38.3	14.1	42.8	146.2

temperature differential in the y-direction than in the z-direction. Figure 4 shows the heat flux profiles for the horizontal pattern at the three primary rates. These plots correspond with the data in Table 3.

Heat Flux Profile for Four Actuators In the previous examination, one probe was placed under an actuator at two locations (first and second probe) and three probes were placed between two actuators. This allowed for higher resolution of the heat flux profile between actuators. Here, one heat flux probe is placed directly under the center of all four actuators, and one probe is placed directly at the midpoint between each actuator. In this section of the study, the odd numbered probes represent the location under the actuators and the even numbered probes are located at the midpoint between actuators.

Looking at the plots in Figure 5, an important pattern emerges immediately. The same heat flux profile exists between all actuators along the centerline. This is significant because it justifies the initial assumption that, at steady state, the same heat flow characteristics are present at all inter-actuator locations. Additionally, this assumption was correct for all patterns and was not an artifact of observing an isolated area. The general trend describes the heat flux difference in y-direction, as probe number increases, magnitude for the horizontal pattern increases, remains approximately the same for the diagonal pattern and decreases in magnitude for the arbitrary pattern.

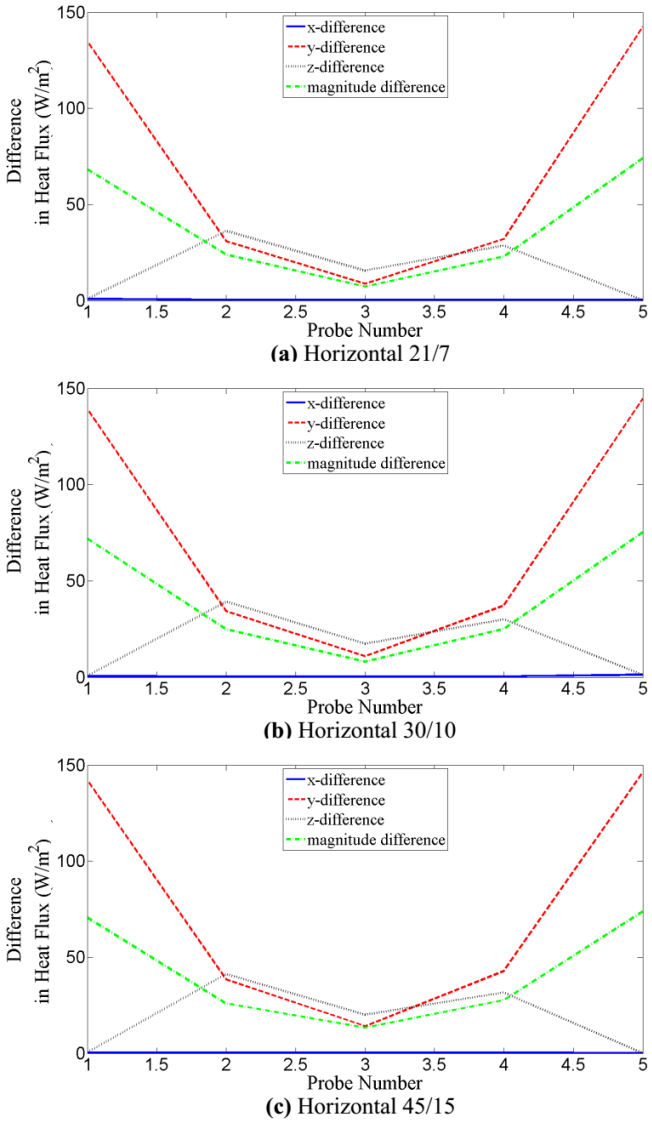

FIGURE 4: Heat flux profiles for Horizontal simulation patterns. (a) is Horizontal 21/7. (b) is Horizontal 30/10. (c) is Horizontal 45/15.

Correlation Between Experiment and Simulation

The primary goal of this study was to develop a relationship between the thermal perception data gathered from the experiments performed by Manasrah et al. [13] with the heat flux data from the simulations. From the experimental data, thermal perception values were determined based on a slightly altered version of the ASHRAE Standard 55 thermal comfort scale. They assigned a number from -3 to +3 where -3 represented cold and and +3 is when subjects felt hot. Intermediary numbers were designed for intensity of thermal feeling.

From the experimental data for the spatial patterns, it was determined that the horizontal pattern was the most effective with a mean thermal sensation value of -0.53. The mean thermal sensation value for the arbitrary pattern was smaller yet not significantly different from the horizontal pattern at -0.50. The diagonal pattern produced a much lower and statistically different average thermal sensation value of -0.38. All spatial patterns were tested using the 30/10 heating/cooling rate.

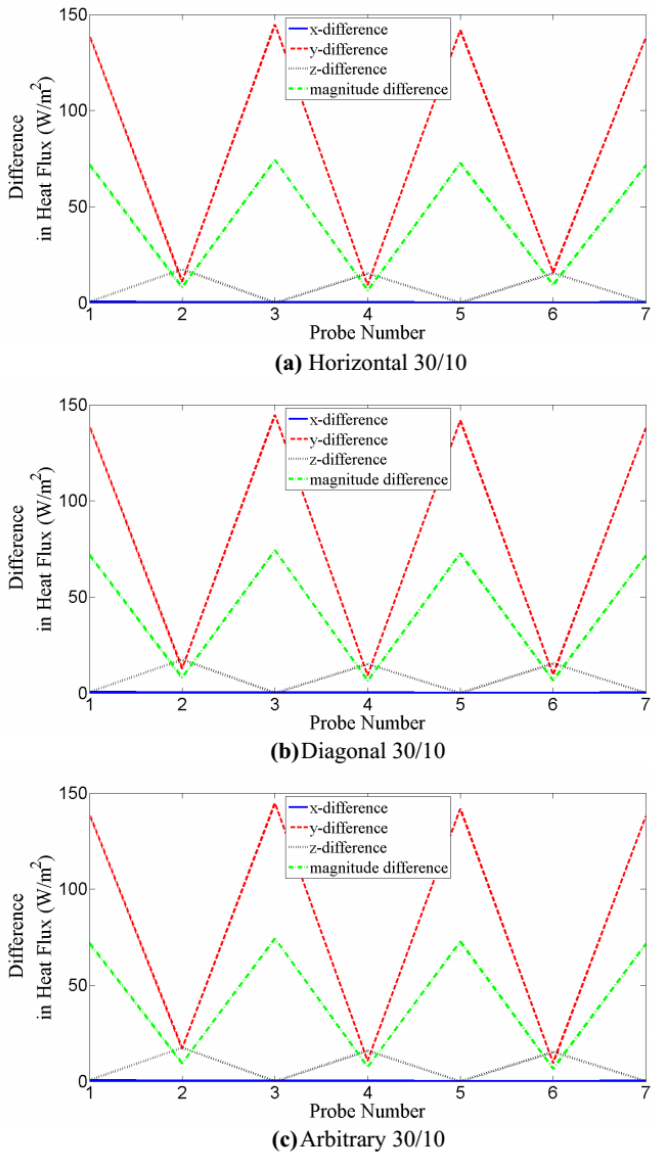

FIGURE 5: Heat flux profile for the three spatial patterns at the 30/10 heating/cooling rate. This image is the heat flux profile for the extended centerline of actuators. Odd numbers represent probes under actuators and even numbers represent the probes between actuators. (a) Horizontal 30/10. (b) Diagonal 30/10. (c) Arbitrary 30/10.

The first analysis of the simulated data involved overlaying the heat flux and temperature plots. The results gained from this did not yield a correlation because the global extreme values for heat flux were very similar. Additionally, the same behavior was exhibited by all patterns. The flux and temperature plots for the x and z directions between actuators were out of phase with each other due to the necessity of heat to propagate before a temperature differential could be apparent. This was observed in all patterns and therefore, no discernible relationship could be concluded.

The second examination involved identifying differences in the heat flux profile between two and four actuators. A range of values were evaluated at all probe locations including: maximum, minimum, average, difference, and percent difference. The heat flux profiles for all pattern combinations yielded very similar results. It was observed that regardless of which spatial pattern, nearly identical heat flux profiles were generated. Additionally, the different heating/cooling rates served only to scale the different patterns and the scaling was, again, nearly identical between patterns.

Perception Metrics and Heat Flux Correlation The thermal perception values listed above were combined in several ways in order to generate a relationship between the patterns. It should be noted that physical experiments for horizontal 21/7, horizontal 45/15, arbitrary 21/7 and arbitrary 45/15 were not performed due to experimental time constraints with each subject.

Perception metrics for these combinations were extrapolated from the the existing data. For simplicity, the spatial pattern metrics will be denoted as "S" and the temporal pattern metrics will be known as "T". Several combinations of these perception metrics were looked at including multiplication of metrics, inverse combination of metrics, and square roots of metrics; some showed promising trends and potential for a relationship with heat flux.

Figure 6a shows that a certain pattern exists from the combination of metrics. For each combination of timing pattern, the diagonal pattern is the most strongly perceived. The 30/10 pattern generated the strongest sensation of cooling except when comparing the horizontal 30/10 combination to the diagonal 21/7 combination.

In order to generate a relationship, the heat flux difference was calculated for all coordinate directions (x, y and z) and the total magnitude is the resultant heat flux, independent of direction. The heat flux difference in the total magnitude value showed the strongest relationship with the actual thermal perception. Figure 6b shows the absolute maximum heat flux difference for the heat flux probes.

To derive a correlation between experimental results and simulation analyses, these two quantities were plotted with perception as a function of heat flux. Equation 8 expresses the relationship between thermal sensation (TS) and heat flux difference (HFD). This relationship shows an R^2 value of 0.76. Each group of three data points has timing pattern in common. This implies that modulation of temporal patterns have a stronger impact on thermal sensation.

$$TS = 0.988 * HFD - 72.50 \quad (8)$$

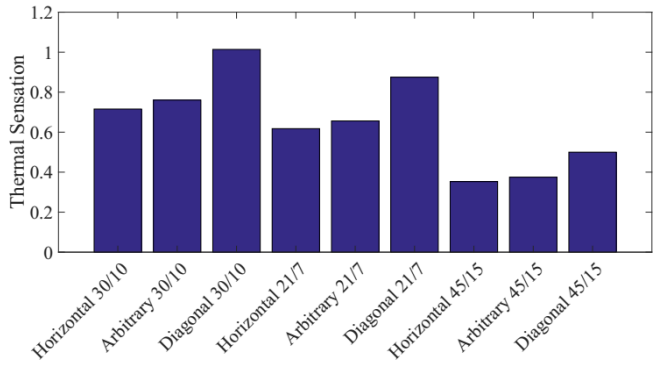

(a) Combined temporal and spatial pattern metrics.

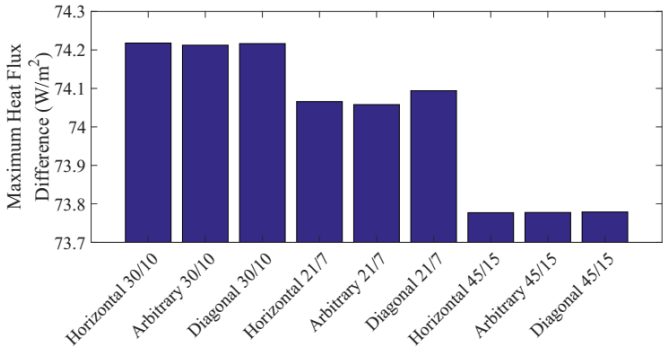

(b) Absolute maximum heat flux difference for probes in the simulation.

FIGURE 6: Comparison between experimental results and corresponding heat flux simulation results.

OPTIMIZING HEATING AND COOLING PATTERNS

It is desirable to increase the effectiveness of the heating and cooling cycles in order to increase the sensation of constant cooling. To achieve this goal a modified pattern was proposed.

Non-Linear Time Patterns

A non-linear thermal pattern is advantageous to a linear pattern since without changing cooling exposure time it increases the heat flux difference which has been proved to be central in perception metric.

For this section of the study, the 30/10 heating/cooling pattern has been modified and applied to the three spatial patterns to see the effects of non-linear cooling. The cooling segment will still consist of decreasing one degree over 10 seconds to maintain the three-to-one ratio. Figure 7 illustrates the non-linear heating/cooling pattern. The heating rate is standard. The cooling segment consists of a 0.75°C drop in temperature in two and a half seconds. This is followed by a 0.15°C drop in temperature over two and a half seconds and finally a 0.1°C drop in temperature for the last over the final 5 seconds. The heat flux difference values were much larger than any of the

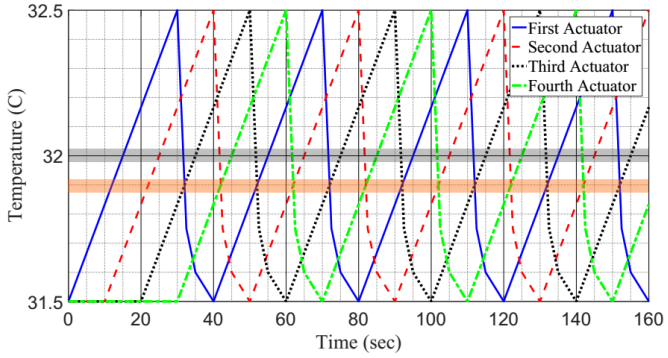

FIGURE 7: The 30/10 non-linear heating/cooling pattern. This pattern consists of the standard heating rate with rapid cooling in order to for the actuator be at a cooler temperature for longer. The red highlight indicates the desired average temperature, 32°C. The yellow highlight shows the average temperature produced by this pattern, 31.9°C.

standard patterns; approximately 14.2% larger than the standard patterns. The heat flux difference values produced by the non-linear pattern were 84.81 W/m^2 for the arbitrary and 84.79 W/m^2 for the diagonal pattern.

CONCLUSIONS

The heat flux characteristics of asymmetrically heating and cooling thermal stimuli have been investigated. Primary contributions of this study include (1) the determination of heat flux values and patterns for different heating and cooling rates, (2) the heat flow patterns present in the thermal display developed by Manasrah et al. [13] have been determined and evaluated, (3) reasons for the effectiveness of different spatial and temporal pattern combinations have been presented, (4) a mathematical relationship between heat flux and thermal perception has been hypothesized and, (5) new and modified patterns have been developed and evaluated to determine their potential effectiveness in producing a cooling sensation.

There seems to be evidence suggesting that the magnitude of heat flux, independent of direction, is the primary factor for thermal sensation. The 30/10 heating/cooling rate produced the strongest sensation followed by the 21/7 pattern and the 45/15 pattern produced the weakest sensation. This is consistent with preliminary findings.

While the resultant magnitude of heat flux was ultimately used to determine a relationship, this magnitude value was heavily influenced by the heat flux values in the radial dimension. This is not surprising due to the fact that the heating source is orthogonal to the medium being heated. Timing rate was the primary factor in differentiating among heat fluxes produced and therefore the effects of perimeter and area seem to be a weaker indicator of thermal sensation.

Future work may help to validate some of the claims made by this research as well as address additional questions not answered by this work. Questions such as at what heat flux values is thermal sensation actually triggered, and whether this sensation remains once triggered or if it gradually fades if not actively maintained. Placing two actuators of different sizes at multiple distances apart and fluctuating temperature could lead to a better understanding of the directional effects of heating and cooling. Similar questions may be asked to determine the subjects' thermal sensation.

ACKNOWLEDGMENT

This material is based upon work supported by the National Science Foundation under Grant Number IIS-1526475.

REFERENCES

[1] T E Finger. Evolution of taste and solitary chemoreceptor cell systems. *Brain, Behavior and Evolution*, 50(4):234–243, 1997.

[2] K. O. Johnson. The roles and functions of cutaneous mechanoreceptors, 2001.

[3] Raf J. Schepers and Matthias Ringkamp. Thermoreceptors and thermosensitive afferents, 2010.

[4] Barry G Green. The effect of skin temperature on vibrotactile sensitivity. *Perception & Psychophysics*, 21(3):243–248, 1977.

[5] Ken Parsons. *Human thermal environments*. 2003.

[6] Joseph C Stevens. Thermal sensibility. In *Psychology of Touch*, pages 61–89. 1991.

[7] D. R. Kenshalo. Correlations of temperature sensitivity in man and monkey, a first approximation. *Sensory functions of the skin with special reference to man*, pages 305–330, 1976.

[8] Barry G. Green. Temperature perception and nociception, 2004.

[9] Didier Bouhassira, Delphine Kern, Jean Rouaud, Emilie Pelle-Lancien, and Françoise Morain. Investigation of the paradoxical painful sensation (illusion of pain) produced by a thermal grill. *Pain*, 114(1):160–167, 2005.

[10] Dan R. Kenshalo, Charles E. Holmes, and Paul B. Wood. Warm and cool thresholds as a function of rate of stimulus temperature change. *Perception & Psychophysics*, 3(2):81–84, 1968.

[11] H Hensel and RD Wurster. Static behaviour of cold receptors in the trigeminal area. *Pflügers Archiv*, 313(2):153–154, 1969.

[12] H Benzing, H Hensel, and R Wurster. Integrated static activity of lingual cold receptors. *Pflügers Archiv European Journal of Physiology*, 311(1):50–54, 1969.

[13] Ahmad Manasrah, Nathan Crane, Rasim Guldiken, and Kyle B Reed. Perceived cooling using asymmetrically-applied hot and cold stimuli. *IEEE Transactions on Haptics*, 10(1):75–83, 2017.

[14] Ahmad Manasrah, Nathan Crane, Rasim Guldiken, and Kyle B. Reed. Asymmetrically-applied hot and cold stimuli gives perception of constant heat. In *World Haptics Conference*, pages 484–489. IEEE, 2017.

[15] Bengt Sundén. *Introduction to heat transfer*. WIT Press, 2012.

[16] Sankaran Mahadevan. Monte carlo simulation. *Mechanical Engineering-New York And Basel-Marcel Dekker*, pages 123–146, 1997.

[17] Daryl L Logan, Evelyn Veitch, Chris Carson, Kamilah Reid Burrell, Vicki Gould, Erin Wagner, Daryl L Logan, Evelyn Veitch, Chris Carson, Kamilah Reid Burrell, Vicki Gould, and Erin Wagner. *A First Course in the Finite Element Method Fourth Edition*, volume 147. 2007.

[18] Il-hwan Seo, In-bok Lee, Oun-kyeong Moon, Se-woon Hong, Hyun-seob Hwang, Jessie P Bitog, Kyeong-seok Kwon, Zhangying Ye, and Jong-won Lee. Modelling of internal environmental conditions in a full-scale commercial pig house containing animals. *biosystems engineering*, 111(1):91–106, 2012.

[19] Patrick M Knupp. Achieving finite element mesh quality via optimization of the Jacobian matrix norm and associated quantities. Part I - a framework for surface mesh optimization. *International Journal for Numerical Methods in Engineering*, 48(January 1999):401–420, 2000.

[20] ANSYS. ANSYS Mechanical APDL Theory Reference. *ANSYS Inc*, Release15(November):1 – 909, 2013.

[21] Ralf Diekmann, Robert Preis, Frank Schlimbach, and Chris Walshaw. Aspect ratio for mesh partitioning. In *Euro-Par98 Parallel Processing*, pages 347–351. Springer, 1998.

[22] MF Bott. Programming and problem solving with ada, 1995.

[23] Saeed Moaveni. *Finite Element Analysis Theory and Application with ANSYS, 3/e*. Pearson Education India, 2008.

[24] Frank P. Incropera, Theodore L. Bergman, Adrienne S. Lavine, and David P. DeWitt. *Fundamentals of Heat and Mass Transfer*. 2011.

[25] DW Hahn and MN Özişik. Heat conduction. hoboken, 2012.